

1 **Allosteric activation of Hsp70 reduces mutant huntingtin levels, the**
2 **clustering of N-terminal fragments, and their nuclear accumulation**

3

4 Brígida R. Pinho^{1,2}, Liliana M. Almeida^{1,2}, Michael R. Duchén^{3,4}, Jorge M. A. Oliveira^{1,2,4}

5

6 ¹UCIBIO-REQUIMTE – Applied Molecular Biosciences Unit, Department of Drug
7 Sciences, Faculty of Pharmacy, University of Porto, Portugal.

8 ²Associate Laboratory i4HB – Institute for Health and Bioeconomy, Department of Drug
9 Sciences, Faculty of Pharmacy, University of Porto, Portugal.

10 ³Department of Cell and Developmental Biology, University College London, London
11 WC1E 6BT, UK.

12 ⁴Consortium for Mitochondrial Research (CfMR), University College London, Gower
13 Street, WC1E 6BT London, UK

14

15 Corresponding authors:

16 Jorge M. A. Oliveira (jorgemao@ff.up.pt) and Brígida R. Pinho (brpinho@ff.up.pt)

17 Departamento de Ciências do Medicamento, Laboratório de Farmacologia, Faculdade
18 de Farmácia, Universidade do Porto

19 Rua de Jorge Viterbo Ferreira, 228, 4050-313 Porto, Portugal

20 Tel. +351 220428610

21

22 **Abstract**

23 Aims: Huntington's disease (HD) is caused by a mutant huntingtin protein that misfolds,
24 yields toxic N-terminal fragments, aggregates, and disrupts proteostasis. The Hsp70
25 chaperone is a potential therapeutic target as it prevents proteotoxicity by favouring
26 protein folding, disaggregation, or degradation. We tested the hypothesis that allosteric
27 Hsp70 activation with a pharmacological mimetic of the Hsp70 co-chaperone Hip, YM-
28 1, could modulate huntingtin proteostasis.

29 Main methods: We used HD cell models expressing either N-terminal or full-length
30 huntingtin. Using single-cell analysis we studied huntingtin aggregation in different
31 cellular compartments by fluorescence microscopy. Protein interaction was evaluated by
32 immunoprecipitation, while protein levels were quantified by immunofluorescence and
33 western-blot.

34 Key findings: N-terminal huntingtin interacted with Hsp70 and increased its levels.
35 Treatment with YM-1 reduced N-terminal huntingtin clustering and nuclear aggregation.
36 Full-length mutant huntingtin also interacted with Hsp70, and treatment with YM-1
37 reduced huntingtin levels when combined with Hsp70 induction by heat shock.
38 Mechanistically, YM-1 increases the Hsp70 affinity for substrates, promoting their
39 proteasomal degradation. Consistently, YM-1 reduced the levels of ubiquitinated
40 proteins. Interestingly, YM-1 accumulated in mitochondria, interfered with its Hsp70
41 isoform involved in protein import, and increased NRF1 levels, a regulator of proteasome
42 genes. We thus suggest that YM-1 may trigger the coordination of mitochondrial and
43 cytosolic proteostasis, enhancing protein degradation.

44 Significance: Our findings show that the strategy of allosteric Hsp70 activation holds
45 potential for HD. While drug efficacy may be limited to tissues with elevated Hsp70,
46 combined therapies with Hsp70 elevating strategies could harness the full potential of
47 allosteric Hsp70 activators for HD.

48

49 **Keywords**

50 Neurodegeneration; Huntington's disease; proteostasis; Hsp70; mitochondria; ubiquitin-
51 proteasome system.

52

53 **Abbreviations**

54 CHIP, C-terminal Hsp70-interacting protein; HD, Huntington's disease; Hip, Hsp70
55 interacting protein; HSF1, heat shock factor 1; Htt, huntingtin; mut-Htt, mutant

56 huntingtin; NRF1, nuclear factor erythroid 2-related factor 1 (not to be confused with
57 nuclear respiratory factor 1); polyQ, polyglutamine.

58 **1. Introduction**

59

60 Huntington's disease (HD) is a neurodegenerative disorder without effective treatment
61 caused by a polyglutamine (polyQ) expansion mutation in the N-terminal region of the
62 huntingtin (Htt) protein [1, 2]. Mutant huntingtin (mut-Htt) is highly prone to
63 fragmentation, which leads to the accumulation of toxic small N-terminal fragments that
64 can misfold and aggregate [2, 3]. Chronic expression of mut-Htt overwhelms the
65 chaperone machinery and protein degradation pathways, inducing the collapse of the
66 proteostasis network [4].

67 Molecular chaperones are key players of the proteostasis network that minimize
68 misfolding and aggregation events [5]. The Hsp70 family, which comprises isoforms with
69 different cellular localizations, promote the folding of newly synthesized proteins,
70 solubilize aggregated proteins and prevent aggregation by refolding misfolded proteins
71 or by cooperating with protein degradation pathways to clear aberrant proteins [6, 7].
72 ATP binding and hydrolysis in the Hsp70 nucleotide-binding domain regulate the
73 interaction of Hsp70 with client proteins: while ATP binding reduces the affinity of the
74 substrate-binding domain to the substrates, ATP hydrolysis into ADP increases the
75 affinity of Hsp70 to the substrates. This nucleotide cycle of Hsp70 is further regulated by
76 co-chaperones, including the Hsp70-interacting protein (Hip) [6, 8, 9]. Hip stabilizes the
77 ADP-bound state, delaying the substrate release. This delay favours the ubiquitination of
78 the Hsp70-bound substrates by the C-terminal Hsp70-interacting protein (CHIP), and
79 targeting for proteasomal degradation [7, 9].

80 Promoting Hsp70 activity through its overexpression or the overexpression of its
81 co-chaperone Hip reduced aggregation of mut-Htt in HD models: Hsp70 overexpression
82 reduced mut-Htt aggregation in cells [10, 11], and in early disease stages of the R6/2 mice
83 [12]; Hip overexpression reduced the size and number of mut-Htt aggregates in cultured
84 cortical neurons expressing N-terminal Htt [13, 14]. The opposite strategy of inhibiting
85 Hsp70 activity, using the ATP-competitive inhibitor VER-155008 [15], accelerated the
86 degeneration of cells expressing mut-Htt [16]. Collectively, these data indicate that
87 strategies that promote the activity of Hsp70, such as the overexpression of Hsp70 or of
88 its co-chaperone Hip, are potential therapeutic strategies in HD.

89 YM-1 is an allosteric activator of Hsp70 that mimics the co-chaperone Hip,
90 favouring the accumulation of the ADP-bound form of Hsp70 [17]. This promotes a
91 longer interaction between Hsp70 and its substrates [17], enhancing CHIP-dependent

92 ubiquitination of the substrates and their proteasomal degradation [7]. Treatment with
93 YM-1 decreased the levels of the mutant-androgen receptor oligomers and aggregates in
94 a cellular model of Kennedy's disease [17], and decreased the levels of the misfolded
95 protein tau in models of tauopathy [18, 19]. It is currently unknown if YM-1 reduces
96 protein aggregation in other misfolding diseases, such as HD.

97 In the present study, we test the hypothesis that Hsp70 allosteric activation with
98 YM-1 may reduce mut-Htt levels and aggregation. As in HD mut-Htt occurs in full-length
99 and in aggregate-prone N-terminal species, and as Hsp70 levels vary with the progression
100 of the disease [12], we test the efficacy of YM-1 in N-terminal and in full-length cellular
101 HD models, with or without heat shock treatment to induce the expression of Hsp70.

102 **2. Materials and Methods**

103

104 **2.1. Cellular models of HD**

105 *N-Terminal Htt model.* Previous studies investigated N-terminal mut-Htt aggregation in
106 transfected U2OS cells [20, 21]. The efficient transfection and the optimal morphological
107 features of U2OS cells - large and flat, allowing imaging markers such as protein
108 aggregates in different compartments - explain their widespread use in neuroscience
109 studies [22, 23]. Here, U2OS cells (ATCC) were grown as we previously described [24],
110 using Dulbecco's Modified Eagle's Medium (DMEM; A1443001, Gibco), supplemented
111 with 10 mM galactose, 5 mM HEPES and 1 mM sodium pyruvate (Sigma-Aldrich), plus
112 2 mM glutamine, 10% fetal bovine serum, and 1% penicillin/streptomycin (Gibco). In
113 order to express the N-terminal Htt fragment, cells were transfected with plasmids
114 encoding either 'wild-type' EGFP-Htt^{ex1}Q23 or 'mutant' EGFP-Htt^{ex1}Q74 (40261 and
115 40262, Addgene), using the Lipofectamine LTX Reagent (Invitrogen) as we previously
116 described [24]. U2OS cells were seeded at 2×10^4 cells/cm² in 13 mm diameter coverslips
117 (Thermo Scientific) and in 6-well plates (TPP) for immunofluorescence and protein
118 extraction, respectively. For live imaging, cells were seeded at 4.5×10^4 cells/cm² in 8-
119 well glass-bottom μ -slides (Ibidi).

120 *Full-length Htt model.* Previous studies investigated the proteostasis of full-length
121 Htt in PC12 cells containing the full Htt transgene, overcoming the low transfection rates
122 of a large gene such as Htt [25, 26]. PC12 cells have also been used to study the effects
123 of Hsp70 modulation on the proteostasis of mutant androgen receptor - another polyQ
124 containing protein [17]. Here, we used PC12 cells with inducible expression of full-length
125 Htt containing 23 (wild-type, CH00285) or 145 (mutant, CH00289) polyQ repeats
126 (Coriell Cell Repository). Cells were cultured in DMEM (2430054, Gibco),
127 supplemented with: 15% horse serum, 2.5% fetal bovine serum, 0.2 mg/ml geneticin, and
128 1% penicillin/streptomycin (Gibco), and with 0.2 mg/ml zeocin (Invivogen). To induce
129 Htt expression, cells were incubated with 5 μ M ponasterone A (Sigma-Aldrich) for 24 or
130 96 h. Cells were seeded at 4.2×10^4 cells/cm² in 6-well plates (TPP) for protein extraction,
131 and at 1.0×10^4 cells/cm² in 13 mm diameter coverslips (Thermo Scientific) for
132 immunofluorescence.

133

134 **2.2. Chaperone modulation**

135 *Pharmacological modulation* - We used YM-1, an allosteric activator of Hsp70 that
136 increases its substrate binding affinity [17]. Previous studies in cell models of tau
137 pathology identified 3 μ M YM-1 as an effective concentration [18]. We measured the
138 concentration-dependent effects of YM-1 on cellular resazurin metabolism, and
139 confirmed 3 μ M as a bioactive concentration without significant toxicity. Cells were thus
140 treated with either solvent (0.1% DMSO) or 3 μ M YM-1 for 24 h: treatment of the N-
141 terminal Htt model started upon completion of the transfection protocol; treatment of the
142 full-length Htt model started 72 h (3 days) after induction of Htt expression. The study of
143 resazurin (Sigma-Aldrich) metabolism was performed as we previously described [24].

144 *Heat shock modulation* - Heat shock was previously used to induce Hsp70 [27].
145 We induced heat shock at 16 h post-treatment (YM-1 or solvent control) by incubating
146 cells for 1 h at 42 °C [28]. Cells were then returned to the standard 37 °C for a 7 h recovery
147 period before protein extraction or immunofluorescence at 24 h post-treatment. To
148 control for the effects of heat shock, we used cells continuously maintained at 37 °C.

149

150 **2.3. Immunoprecipitation and western blot**

151 *Protein extraction and quantification* - was performed as we previously described [29].
152 Cells were rinsed with ice-cold phosphate-buffered saline (PBS) and lysed in buffer (pH
153 = 7.4) containing 50 mM Tris (NZYTech), 150 mM NaCl (Merck), 1 mM EDTA, 1%
154 IGEPAL CA-630, 1% sodium deoxycholate, 0.1% sodium dodecyl sulfate (Sigma-
155 Aldrich), and protease inhibitor cocktail (Thermo Scientific). After homogenization with
156 Precellys® Evolution (5800 rpm, 2 x 15 s and pauses of 30 s) and 3 freeze-thaw cycles,
157 the lysates were centrifuged at 600 x g, for 10 min, at 4°C. Supernatant protein
158 concentrations were quantified via the Bradford method (Bio-Rad).

159 *Immunoprecipitation.* SureBeads™ Protein G Magnetic Beads (Bio-Rad) were
160 incubated with either anti-Hsp70 (PA5-28003, Invitrogen; 1:500 for 10 min) or anti-GFP
161 (MA5-15256, Invitrogen; 1:200 for 30 min) – to selectively immunoprecipitate N-
162 terminal Htt from the transfected cells. After washing (PBS with 0.1% Tween 20; Sigma-
163 Aldrich), SureBeads were incubated with test samples containing 500 μ g of protein for 1
164 h [29]. After 3 washes, bound proteins were eluted in NuPAGE LDS sample buffer
165 (Invitrogen), for 10 min at 70°C, and then processed for western blot.

166 *Western blot.* Samples were denatured at 70 °C for 10 min (in NuPAGE LDS
167 buffer supplemented with NuPAGE reducing agent; Invitrogen), loaded (20-25 μ g
168 protein) into polyacrylamide gels (3-8 % Tris-acetate or 4-12 % Bis-Tris NuPAGE

169 precast gels, Invitrogen), electrophoresed (150 V, 50 min for 3-8 % gels; 200 V, 30 min
170 for 4-12 % gels), and electro-blotted to PVDF membranes (25 V for 6-8 min; iBlot-2 dry
171 blotting system; Invitrogen). Membranes were blocked with 5 % bovine serum albumin
172 (BSA, NZYTech) in PBS with 0.05 % Tween 20, then incubated with primary and
173 respective secondary antibodies. Primary antibodies: anti-Htt-NT (1:500; 4-19 N-
174 terminal; CH00146, Coriell Institute), anti-polyQ (1:3000; anti-polyQ clone 5TF1-1C2;
175 MAB1574, Merck Millipore), anti-ubiquitin (1:1000; sc-8017, Santa Cruz
176 Biotechnology), anti-Hsp70 (1:1000; sc-66049, Santa Cruz Biotechnology / 1:3000; PA5-
177 28003, Invitrogen), and anti-Grp75 (1:1000; mitochondrial Hsp70; sc-133137, Santa
178 Cruz Biotechnology). Secondary antibodies (Invitrogen): horseradish peroxidase-
179 conjugated anti-mouse (1:4000, G-21040) and anti-rabbit (1:4000, G-21234). Detection
180 was performed using Novex ECL Chemiluminescent kit (Invitrogen) and a Chemidoc
181 MP imager (Bio-Rad). Membranes were stained with coomassie for protein loading
182 control.

183

184 **2.4. Fluorescent probes and Immunolabeling**

185 To label polarized mitochondria and indirectly evaluate the mitochondrial membrane
186 potential with single-cell resolution microscopy, cells were incubated (30 min at 37 °C)
187 with 10 nM TMRM⁺ (Invitrogen) - before live imaging; or with 300 nM MitoTracker
188 Deep Red (Invitrogen) - before fixation. To label nuclei/DNA, cells were incubated with
189 5 µg/ml Hoechst 34580 (Sigma-Aldrich) for 5 min and washed in PBS. For
190 immunolabeling, cells in coverslips were fixed with 4 % paraformaldehyde for 15 min at
191 37 °C, washed in PBS, and permeabilized and blocked with 0.1 % Triton X-100 (Sigma-
192 Aldrich) and 3 % BSA in PBS for 30 min. Cells were then incubated with primary
193 antibody for 1 h at room temperature or overnight at 4 °C: anti-GFP (1:2000; MA5-15256,
194 Invitrogen); anti-Htt-NT (1:200; CH00146, Coriell Institute), anti-Hsp70 (1:200; PA5-
195 28003, Invitrogen); anti-Grp75 (1:200; 14887-1-AP, Proteintech); and anti-Hsp90
196 (1:200; sc-13119, Santa Cruz Biotechnology). Cells were then washed with 0.1 % Triton
197 X-100 in PBS and incubated for 1 h with the respective AlexaFluor-488 (anti-mouse, A-
198 11029) and -568 (anti-rabbit, A-11036) conjugated secondary antibodies (1:200;
199 Invitrogen). Coverslips were then assembled in a fluorescent mounting medium (Dako).

200

201 **2.5. Fluorescence microscopy**

202 Image acquisition was performed using non-saturating identical equipment settings to
203 allow intensity comparisons between treatments. Images were acquired in an inverted
204 microscope (Eclipse TE300, Nikon) with a motorized stage (ProScan, Prior), a
205 monochromator (Polychrome II, Photonics), and a CCD camera (ORCA-ER,
206 Hamamatsu), all controlled by the Micro-Manager 2.0 software [24]. Additionally, high-
207 resolution images were acquired using an inverted confocal laser scanning microscope
208 with Airyscan processing (Zeiss, LSM 880). AlexaFluor-488 and EGFP were excited at
209 488 nm, AlexaFluor-568 and TMRM⁺ at 557 nm, MitoTracker Deep Red at 640 nm, and
210 Hoechst 34580 at 380 nm. YM-1 fluorescence was detected with excitation at 488 and
211 525 nm. Emissions were collected using band pass filters (Chroma) for DAPI (Hoechst),
212 FITC (EGFP, AlexaFluor-488, YM-1), TRITC (TMRM⁺, AlexaFluor-568, YM-1), and
213 CY5 (MitoTracker Deep Red).

214

215 **2.6. Image processing and data analysis**

216 Image background subtraction and densitometric analyses of immunoblots were
217 performed with ImageJ (<http://rsbweb.nih.gov/ij/>; National Institutes of Health). The
218 analyses of U2OS cell images were automated in CellProfiler 3.1.8
219 (<https://cellprofiler.org>; Broad Institute) to identify: transfected cells and huntingtin
220 aggregates (GFP staining); cell compartments (nucleus – Hoechst staining; cytoplasm –
221 Mitotracker Deep Red staining); and extract quantitative measurements of intensity and
222 shape. Aggregates were detected inside cells as GFP-containing particles with a minimum
223 diameter of 2.75 μm . Classification of Htt-GFP expressing cells into ‘diffuse’ or
224 ‘aggregated’ was performed with machine-learning in CellProfiler Analyst 2.2.1. Data
225 calculations were performed with pivot tables (Excel, Microsoft). Graphical
226 representations and statistical analysis were performed with Prism 8.0 (GraphPad
227 Software) or R (<https://www.r-project.org>). The Shapiro-Wilk normality test was used to
228 assess data distributions. Comparisons between two groups were performed using *t*-test.
229 Single-factor analyses were performed using One-Way ANOVA with Dunnett’s (vs.
230 control) or Sidak’s (between groups) post-Hoc tests. Multifactorial analyses (two- or
231 three-way ANOVA) were used to test interactions and main effects of the different
232 factors. Correlation analyses were performed with the linear model function in R. For all
233 analyses, a *P* value under 0.05 was taken as statistically significant. Unless otherwise
234 stated, data are mean \pm standard error of the mean (SEM), or median and interquartile
235 range (boxplots), of at least 3 independent experiments (*n* specified in figure legends).

236 Analysis of imaging data involved a minimum of 50 cells per condition in each
237 independent experiment.

238

239 **3. Results**

240

241 **3.1. N-terminal huntingtin species interact with Hsp70 and increase its levels**

242 Hsp70 chaperones are key players in cellular proteostasis. They interact with misfolded
243 proteins, promoting their correct folding or degradation, and preventing aggregation [7,
244 9]. To evaluate Hsp70 chaperone levels in the N-terminal Htt cellular model, we
245 quantified protein expression by immunofluorescence. Specifically, we quantified: the
246 cytosolic and nuclear Hsp70 (hereafter referred collectively as ‘Hsp70’ - a combination
247 of constitutive Hsc70 and stress-inducible Hsp72 with over 80% identity; [30]); the
248 mitochondrial Hsp70 isoform (hereafter referred to as ‘Grp75’); and the associated levels
249 of either wild-type or mutant N-terminal Htt (Fig. 1). Hsp70 presented a nuclear and
250 cytosolic distribution (Fig. 1Ai), whereas Grp75 presented a selective mitochondrial
251 distribution: Grp75 presented a cellular distribution similar to the mitochondrial probe
252 MitoTracker (Fig. 1Aii). Using single-cell analysis of cells expressing either wild-type or
253 mutant N-terminal Htt species, we found that the levels of N-terminal Htt positively
254 correlated with Hsp70 levels (Fig. 1B). Overall, Hsp70 levels were significantly elevated
255 in cells expressing N-terminal Htt species vs. control (Fig. 1C). This induction effect was
256 selective for Hsp70, as shown by the unaltered levels of Grp75 (Fig. 1B), and prompts
257 the hypothesis that the N-terminal Htt species interact with Hsp70. Consistently, Hsp70
258 co-immunoprecipitated with either wild-type or mutant N-terminal Htt (Fig. 1D). Thus,
259 in this HD cellular model, the N-terminal Htt species interact with Hsp70 and this is
260 associated with a compensatory increase in the levels of this chaperone.

261

262 **3.2. Mutant N-terminal huntingtin aggregates recruit Hsp70**

263 To characterize the interaction between N-terminal mut-Htt and Hsp70, we investigated
264 the spatial distribution of mut-Htt aggregates and its association with Hsp70. Cells
265 expressing mutant N-terminal Htt formed aggregates in the nucleus and cytosol, which
266 were surrounded by a more intense pattern of Hsp70 distribution than areas without
267 aggregates (Fig. 2A, B). In contrast, the other major cellular chaperone – Hsp90 – was
268 not particularly enriched in the vicinity of aggregates (Fig. 2A), indicating that mut-Htt
269 aggregates selectively recruit Hsp70. Additionally, the levels of Hsp70 (Fig. 2Ci) and the
270 heterogeneity of its distribution (Fig. 2Cii) were significantly higher in cells presenting
271 mut-Htt aggregates vs. those expressing only diffuse mut-Htt. Taken together, these
272 results show that Hsp70 interacts with mutant N-terminal Htt, being recruited into

273 aggregates, and suggesting that the allosteric activation of Hsp70 could potentially affect
274 aggregate formation or their cellular distribution.

275

276 **3.3. YM-1 decreases mutant N-terminal huntingtin levels in aggregates and their** 277 **nuclear accumulation**

278 Before examining the effects of the allosteric Hsp70 activator YM-1 on Htt proteostasis,
279 we confirmed YM-1 bioactivity and cellular internalization (taking advantage of YM-1
280 autofluorescence [31]). YM-1 was bioactive, evoking a concentration-dependent
281 decrease in resazurin metabolism (Fig. 3A). The previously reported effective
282 concentration of 3 μ M YM-1 for Hsp70 modulation [18] induced a minor decrease in
283 metabolism (~20%) (Fig. 3Aii) without detectable toxicity (cells maintain normal
284 morphology, mitochondrial polarization, and nuclear integrity; Fig. 3B, C). 3 μ M YM-1
285 was internalized by live cells, where YM-1 autofluorescence overlapped with that of the
286 mitochondrial membrane potential sensitive probe TMRM⁺ (Fig. 3B), consistent with the
287 cation YM-1 accumulating in the negatively charged mitochondria. We thus used 3 μ M
288 YM-1 [18] in all our subsequent experiments, fixing cells after the treatments, and
289 permeabilizing with Triton X-100 to allow antibody penetration and eliminate YM-1
290 autofluorescence, while maintaining nuclear staining with Hoechst (Fig. 3C) and
291 allowing the detection of huntingtin-GFP or MitoTracker Deep Red (Fig. 4D).

292 We next investigated whether treatment with YM-1 influenced the levels of
293 Hsp70, using heat shock as a positive control for Hsp70 induction [27]. Heat shock
294 treatment significantly elevated Hsp70, whereas YM-1 alone maintained Hsp70 levels
295 (Fig. 4A). Given that YM-1 accumulates in mitochondria, we tested if it affected the
296 mitochondrial Grp75 levels, and the MitoTracker Deep Red intensity, which is indicative
297 of mitochondrial levels and polarization status [32]. Treatment with YM-1 significantly
298 elevated Grp75 (Fig. 4B), without detectable changes in MitoTracker Deep Red intensity
299 (Fig. 4C, D).

300 To test the efficacy of YM-1 in promoting protein degradation, we quantified the
301 levels of ubiquitinated proteins in cells expressing mutant N-terminal Htt. Treatment with
302 YM-1 significantly decreased the levels of ubiquitinated proteins (Fig. 5A), suggesting
303 increased proteasome-mediated degradation. We also investigated whether YM-1
304 treatment increases the expression of nuclear factor erythroid 2-related factor 1 (NRF1;
305 not to be confused with nuclear respiratory factor 1), a master transcription factor of
306 proteasome genes [33]. YM-1 treatment increased the levels of NRF1 in cells expressing

307 mutant N-terminal Htt ([Supplementary Fig. 1](#)), suggesting that YM-1 triggers a
308 transcriptional response involving NRF1, promoting protein clearance by the ubiquitin-
309 proteasome system.

310 As results suggest that YM-1 promotes protein degradation, we tested the effects
311 of YM-1 upon mut-Htt aggregation. Cells expressing mutant N-terminal Htt continued to
312 form aggregates when treated with YM-1. However, YM-1 significantly decreased the
313 levels of Htt in the aggregates (reduction of the Htt staining intensity in the aggregates,
314 [Fig. 5B, C](#)), and reduced the proportion of aggregates found in the nucleus ([Fig. 5D](#)). This
315 reduction of nuclear aggregates seems critically dependent on the allosteric activation of
316 Hsp70 with YM-1. Indeed, although heat shock alone suffices to induce Hsp70 ([Fig. 4A](#)),
317 heat shock only reduces the proportion of nuclear aggregates when combined with YM-
318 1 ([Fig. 5D - Heat Shock](#)). Moreover, as there was a corresponding increase in the
319 proportion of cytosolic aggregates ([Fig. 5D](#)), these data suggest that allosteric Hsp70
320 activation with YM-1 retains mut-Htt in the cytosol, reducing its accumulation and
321 aggregation in the nucleus.

322 Taken together, these findings indicate that treatment with the allosteric Hsp70
323 activator YM-1 increases NRF1 levels, promotes protein degradation and modifies the
324 proteostasis of mutant N-terminal Htt, leading to aggregates with lower mut-Htt levels
325 (less compact), and reducing their formation in the nucleus. The YM-1 internalization in
326 mitochondria and the interference with Grp75-dependent protein import may explain
327 increased NRF-1 levels [[33](#), [34](#)], enhancing proteasomal capacity and thus protein
328 degradation. We next investigated whether and how treatment with YM-1 influenced the
329 proteostasis of full-length Htt, in a cellular model without aggregation.

330

331 **3.4. YM-1 lowers mutant full-length huntingtin levels when Hsp70 is induced by heat** 332 **shock**

333 To investigate whether YM-1 also modulates full-length Htt proteostasis, we tested YM-
334 1 in a full-length HD model: cells with ponasterone A-inducible wild-type or mutant full-
335 length Htt expression. After induction with ponasterone A, wild-type and mutant Htt
336 expression increased over time, without formation of mut-Htt aggregates ([Fig. 6A, B](#)). In
337 this full-length HD cell model, cells expressing mut-Htt presented higher levels of Hsp70,
338 while cells expressing wild-type Htt presented similar levels of Hsp70 to non-induced
339 cells ([Fig. 6C](#)). Accordingly, only mut-Htt co-immunoprecipitated with Hsp70 ([Fig. 6D](#)),
340 indicating that the mutant full-length Htt interacts with Hsp70, increasing its levels.

341 Similar to the N-terminal HD model, heat shock treatment increased the levels of
342 Hsp70 in the full-length HD model (Fig. 7A, B). In cells expressing wild-type full-length
343 Htt, YM-1 did not change the levels of ubiquitinated proteins or wild-type Htt (Fig. 7A,
344 C, D). In cells expressing mutant full-length Htt, YM-1 reduced the levels of ubiquitinated
345 proteins when cells were also subjected to heat shock treatment (Fig. 7A, C), which was
346 the condition with the highest level of Hsp70 expression (Fig. 7B). Together with the
347 reduction in ubiquitinated proteins, YM-1 treatment also decreased the levels of mutant
348 full-length Htt (Fig. 7A, E). The key findings and proposed mechanisms are summarized
349 in Fig. 8.

350 4. Discussion

351

352 The pathophysiology of HD is predominantly associated with a toxic gain-of-function of
353 mut-Htt, which has a widespread distribution in the organism. Therapeutic strategies that
354 decrease mut-Htt may benefit HD patients [2, 35]. Such strategies involve reducing mut-
355 Htt production or increasing its clearance. Genetic approaches to reduce mut-Htt
356 production have been tested in clinical trials, with a set of challenges related to invasive
357 drug delivery to the central nervous system [1, 36]. Small molecule drugs that interact
358 with key players of the proteostasis network and promote mut-Htt clearance constitute
359 alternative or complementary therapeutic strategies for HD [37].

360 Htt is a client protein of Hsp70 [38, 39], which supports the study of Hsp70
361 modulation in HD [9]. Here we show that the N-terminal and full-length mut-Htt species
362 expressed by the cellular HD models interact as clients with Hsp70 and increase its levels.
363 Mechanistically, competition with increased client proteins releases the heat shock factor
364 1 (HSF1) from the latency control of Hsp70. Free HSF1 promotes the expression of
365 Hsp70, in a compensatory feedback that protects cells from proteotoxic stress [40-43].
366 However, increasing Hsp70 levels may be insufficient to attenuate Htt proteotoxicity,
367 particularly in advanced HD stages with a high misfolded protein load [44, 45], or the
368 compensatory feedback may fail in cases of low HSF1 levels or activity [40, 46, 47]. This
369 led us to investigate strategies to potentiate the activity of Hsp70, namely its allosteric
370 activation.

371 Our data show that treatment with the Hsp70 allosteric activator YM-1 decreased
372 the levels of full-length mut-Htt. YM-1 also reduced the clustering of N-terminal mut-Htt
373 and the accumulation of aggregates in the nucleus. Mechanistically, YM-1 mimics the
374 co-chaperone Hip [17, 48] increasing the affinity of Hsp70 for client proteins, which
375 delays their release and enhances their ubiquitination by CHIP. Htt presents N-terminal
376 lysine residues - mainly K6 and K9 - that can undergo the ubiquitination that targets Htt
377 for proteasomal degradation [49, 50], decreasing its levels.

378 Regarding Htt aggregation, we propose that YM-1 reduces the levels of N-
379 terminal mut-Htt in aggregates by preventing aggregation or promoting disaggregation.
380 YM-1 can prevent aggregation by activating Hsp70 and thus prolonging its interaction
381 with mut-Htt. Activated Hsp70 can promote disaggregation in cooperation with other
382 chaperones that assemble a disaggregase complex [7]. Treatment with YM-1 also reduced
383 the proportion of nuclear aggregates, which are linked with transcriptional dysregulation

384 [51]. Mechanistically, YM-1 retains mut-Htt in the cytosol through the binding to Hsp70.
385 This retention by Hsp70 also predicts a reduction in the mut-Htt that is available to
386 interact with nucleoporins and disrupt nuclear integrity [52, 53], thereby reducing mut-
387 Htt access to and aggregation in the nucleus.

388 Mitochondria may have a role in the effects of YM-1. Although YM-1 is prevalent
389 in cytosolic fractions [31], its cation nature predicts the internalization of YM-1 in the
390 electronegative environment of mitochondria. Indeed, we show that YM-1 accumulates
391 in mitochondria and increases the levels of the local Hsp70 isoform (Grp75) - a likely
392 feedback response to Grp75 inhibition. Grp75 integrates the translocase of the inner
393 mitochondrial membrane, contributing to the import and folding of nuclear-encoded
394 mitochondrial proteins [54]. The binding of YM-1 to Grp75 may stabilize the ADP-bound
395 form of this chaperone, delaying the release and import of substrates. Perturbations to
396 mitochondrial protein import can trigger a transcriptional response that enhances
397 proteasomal capacity and restores proteostasis, as shown in yeast and mammalian cells
398 [34, 55]. In yeast, this response is mediated by the transcription factor Rpn4, in a
399 protective process called UPR^{am} (*unfolded protein response activated by mistargeting of*
400 *proteins*) [34, 56]. In mammals, a similar process may be mediated by NRF1 (nuclear
401 factor erythroid 2-related factor 1; not to be confused with nuclear respiratory factor 1),
402 which executes comparable functions to Rpn4 as a master transcription factor of
403 proteasome genes [33, 34, 57]. We thus propose that mitochondria-localized YM-1 may
404 trigger a pathway that enhances proteasomal capacity, explaining the associated decrease
405 in ubiquitinated proteins, and contributing to mut-Htt clearance. YM-1 could thus be a
406 valuable pharmacological tool to investigate the currently emerging topic of inter-
407 coordination of cytosolic and mitochondrial proteostasis.

408 Notwithstanding a potential mitochondrial-dependent contribution, the primary
409 effects of YM-1 are dependent on Hsp70 levels. The dependency on Hsp70 levels was
410 also reported for the co-chaperone Hip, which only facilitated protein refolding when co-
411 overexpressed with Hsp70 [14]. Thus, Hsp70 levels are a predictive factor for the efficacy
412 of Hip mimetic allosteric activators such as YM-1. As the levels of chaperones differ
413 among organs and tissues affected by HD, YM-1 may be more potent in tissues with high
414 levels of Hsp70 such as muscle, or when combined with Hsp70 elevating treatments such
415 as Hsp90 inhibition [58, 59].

416

417 **5. Conclusion**

418

419 Here we show that allosteric Hsp70 activation with YM-1 reduces full-length mut-Htt
420 levels, and the clustering and nuclear aggregation of its N-terminal fragments. These
421 findings extend previous knowledge of YM-1 effects on misfolding diseases, being tested
422 here for the first time in HD models. Mechanistically, we propose that YM-1 increases
423 the retention of mut-Htt by Hsp70, favouring its ubiquitination and proteasomal
424 degradation. Additionally, we show that YM-1 targets mitochondria, where its interaction
425 with the mitochondrial Hsp70 may interfere with the protein import to mitochondria,
426 triggering a transcriptional response via NRF1 and activating protein clearance
427 machinery. We propose that YM-1 could be an interesting pharmacological tool to
428 investigate the coordination between mitochondrial and cytosolic proteostasis. As our
429 results suggest that Hsp70 levels are a predictive factor of YM-1 efficacy, combined
430 therapies with Hsp70 elevating strategies will likely be necessary to harness the full
431 potential of allosteric Hsp70 activators.

432

433

434 **Declaration of Competing Interest**

435 The authors declare that they have no conflicts of interest.

436

437 **Acknowledgements**

438 This work was supported by European Union (FEDER funds through COMPETE POCI-
439 01-0145-FEDER-016577) and by Fundação para a Ciência e a Tecnologia (FCT, National
440 funds through the projects P2020-PTDC/NEU-NMC/0412/2014 (3599-PPCDT, PI:
441 JMAO), LA/P/0140/2020 (i4HB), UIDP/04378/2020 and UIDB/04378/2020 (UCIBIO-
442 REQUIMTE). BRP acknowledges FCT for funding through program DL 57/2016 -
443 Norma transitória (DL57/2016/CP1346/CT0016).

444 The authors acknowledge all current and former Lab members for technical assistance
445 with routine Lab work or data discussion in Lab meetings.

446

447 **Figure Legends**

448

449 **Figure 1. N-terminal huntingtin species interact with Hsp70 and increase its levels.**

450 Data are from U2OS cells at 24 h post-transfection with N-terminal Htt constructs: wild-
451 type (wt-Htt; EGFP-Htt^{ex1}Q23) or mutant (mut-Htt; EGFP-Htt^{ex1}Q74). **(A)**
452 Representative immunofluorescence showing nuclei (*blue*; Hoechst); N-terminal Htt in
453 diffuse or aggregated form (*green*; AlexaFluor-488); mitochondria (*magenta*;
454 MitoTracker Deep Red); and Hsp70 (*i - top*) or Grp75 (*ii - bottom*; mitochondrial Hsp70)
455 in red (AlexaFluor-568). **(B)** Correlation analysis between the immunofluorescence
456 intensity levels of N-terminal Htt (*i* - wild-type; *ii* - mutant) and Hsp70 (*red line*) or Grp75
457 (*black line*); a.f.u. - arbitrary fluorescence units; **P* < 0.05, *n* = 200 cells per condition,
458 from 4 independent experiments. **(C)** Immunofluorescence quantification: Hsp70 levels
459 in cells expressing wt- or mut-Htt (*grey bars*) in percentage of control (*white bar*, without
460 N-terminal Htt); **P* < 0.05, *n* = 4 independent experiments, each with ≥ 50 cells per
461 condition. **(D)** Western blots of complete protein samples (Input; *left*) and
462 immunoprecipitated samples (IP; *right*; Pull-down with anti-GFP). Note that: anti-Htt-
463 NT detects N-terminal wt-Htt, whereas anti-polyQ detects N-terminal mut-Htt; Hsp70
464 co-immunoprecipitates with both N-terminal Htt species.

465

466 **Figure 2. Mutant N-terminal huntingtin aggregates recruit Hsp70.**

467 Data are from U2OS cells at 24 h post-transfection with the mutant N-terminal Htt
468 construct (EGFP-Htt^{ex1}Q74). **(A)** High-resolution immunofluorescence imaging of
469 chaperones (Hsp70 or Hsp90; *red*) and mutant Htt aggregates (*green*) - shown with either
470 full dynamic range (non-saturating) or partial dynamic range (to visualize fainter
471 staining); white-dashed lines depict the nuclear borders; note how Hsp70 (but not Hsp90)
472 levels increase specifically in the proximity of nuclear and cytosolic aggregates. **(B)**
473 Representative images of a cell with aggregates (*green*) and Hsp70 immunofluorescence
474 (*red*) along the Z axis - depth (*i*); the dashed line labeled X was used to derive fluorescence
475 intensity profiles (*ii*); note how Hsp70 levels increase in proximity to aggregates. **(C)**
476 Quantification of Hsp70 levels in cells expressing only diffuse N-terminal Htt (Diff; grey
477 bars) vs. cells containing aggregates (Aggr; black bars); *n* = 4 independent experiments,
478 each with ≥ 50 cells; **P* < 0.05. Note that cells with aggregates show higher Hsp70 levels
479 (*i*) with higher heterogeneity due to recruitment (*ii*; higher SD/mean).

480

481 **Figure 3. YM-1 shows concentration-dependent bioactivity and mitochondrial**
482 **localization.**

483 (A) Chemical structure of the Hsp70 allosteric activator YM-1 (i); concentration-
484 dependent effects of YM-1 on resazurin metabolism of U2OS cells (ii); data are mean \pm
485 SD in % control (solvent-treated cells). (B) Live imaging of U2OS cells transfected with
486 the EGFP-Htt^{ex1}Q23 (green) and treated with YM-1 (3 μ M, 24 h), and then incubated
487 with the mitochondrial membrane potential indicator TMRM⁺ (10 nM; red) for 30 min;
488 Note that in cells incubated with TMRM⁺ without YM-1 (solvent control) there is red
489 TMRM⁺ fluorescence (mitochondria), but no green fluorescence in non-transfected cells.
490 When YM-1 is present, there is a green YM-1 autofluorescence in all cells, which
491 overlaps with the red signal of TMRM⁺ (mitochondria). (C) Representative images of
492 U2OS cells treated with solvent or 3 μ M YM-1 (without TMRM⁺), imaged with 488 and
493 525 nm excitation to detect YM-1 autofluorescence in the green and red emission filters;
494 note that permeabilization (0.1% Triton X-100, 30 min) completely removes the YM-1
495 green/red signals, while maintaining the nuclear staining with Hoechst (blue).

496

497 **Figure 4. Heat shock increases Hsp70, whereas YM-1 increases Grp75 levels.**

498 Data are from immunofluorescence assays with U2OS cells expressing wild-type (wt-
499 Htt) or mutant (mut-Htt) N-terminal Htt, treated with solvent (white bars) or YM-1 (3
500 μ M; blue bars), with or without heat shock (42 °C, 1 h), as described in the Chaperone
501 modulation section of Materials & Methods. (A) Hsp70 levels. (B) Grp75 - mitochondrial
502 Hsp70 - levels. (C) MitoTracker Deep Red intensity levels - indicative of mitochondrial
503 levels and polarization status; $n = 4$ independent experiments, each with ≥ 50 cells per
504 condition. Factorial ANOVA: * $P < 0.05$, heat shock effect; # $P < 0.05$, YM-1 effect; \$ $P <$
505 0.05, mut-Htt effect. (D) Representative images of Grp75 immunolabeling and
506 MitoTracker staining in cells expressing N-terminal wt-Htt treated with solvent or 3 μ M
507 YM-1.

508

509 **Figure 5. YM-1 decreases the levels of ubiquitinated proteins, mutant N-terminal**
510 **huntingtin levels in aggregates and their nuclear accumulation.**

511 Data are from U2OS cells expressing mutant N-terminal Htt, treated with solvent or YM-
512 1 (3 μ M; blue color), with or without heat shock (42 °C, 1 h), as described in the
513 Chaperone modulation section of Materials & Methods. (A) Ubiquitinated-proteins: (i)
514 ubiquitinated proteins levels - in percentage of cells treated with solvent - quantified by

515 western blot; **(ii)** representative blot; $n = 5$ independent experiments; $*P < 0.05$. **(B)**
516 Representative image of cells showing mutant Htt (green) in diffuse form or aggregated;
517 white-dashed lines delimit nuclei; arrows signal representative aggregate locations:
518 nuclear, cytosolic, or in the nuclear-cytosolic interface. **(C)** Htt levels in aggregates
519 quantified by the intensity of Htt staining (anti-GFP) by immunofluorescence - in
520 percentage of the Htt levels from cytosolic aggregates of control cells (treated with
521 solvent, without heat shock); $*P < 0.05$ vs. respective aggregates in control cells; the left-
522 pointing arrows denote that the boxplots in the heat shock condition (right) are
523 statistically compared with the boxplots in the control condition (left; solvent without
524 heat shock). **(D)** Proportion of aggregates per location: cytosolic, nuclear, or nuclear-
525 cytosolic interface; $*P < 0.05$, effect of YM-1 vs. solvent. **(C, D)** Data are from 4
526 independent experiments, each with ≥ 50 cells per condition.

527

528 **Figure 6. Mutant full-length huntingtin interacts with Hsp70 and increases its levels.**

529 Data are from inducible PC12 cells expressing full-length huntingtin (wild-type: wt-Htt;
530 mutant: mut-Htt). **(A-i)** Protocol: cells were treated with either solvent (control) or
531 inducer (ponasterone A) for 4 days before protein extraction (a 1 day induction condition
532 was included to assess the time-dependence of Htt expression). **(A-ii)** Representative
533 immunofluorescence images of cells with anti-Htt-NT (green) and nuclei (blue) at 4 days
534 post-induction. **(A-iii)** Representative western blots with anti-Htt-NT (stronger
535 recognition of wt-Htt), anti-polyQ (stronger recognition of expanded polyQ in mut-Htt),
536 and anti-Hsp70; Coomassie: loading control. **(B)** Levels of **(i)** wt- and **(ii)** mut-Htt,
537 respectively quantified with anti-Htt-NT and anti-polyQ by Western Blot, at 1 and 4 days
538 post-induction. $n = 4$ independent experiments. **(C)** Levels of Hsp70 quantified by
539 western blot in control (non-induced; white bar) vs. induced cells (grey bars) at 4 days
540 post-induction; $n = 4$ independent experiments; $*P < 0.05$ vs. control. **(D)** Western blots
541 of complete protein samples (Input; *left*) and immunoprecipitated samples (IP; *right*; Pull-
542 down with anti-Hsp70); note that Hsp70 co-immunoprecipitated with full-length mut-Htt
543 (detected with anti-polyQ), but not with wt-Htt (detected only in the Input with anti-Htt-
544 NT).

545

546 **Figure 7. YM-1 decreases mutant full-length huntingtin and ubiquitinated proteins**
547 **when Hsp70 is induced by heat shock.**

548 Data are from induced PC12 cells expressing full-length huntingtin (wild-type: wt-Htt;
549 mutant: mut-Htt). Htt expression was induced with ponasterone A for 4 days; at 3 days
550 post-induction, cells were treated with solvent or YM-1 (3 μ M) for 24 h, with or without
551 heat shock (42 $^{\circ}$ C, 1 h), as described in the Chaperone modulation section of Materials &
552 Methods. **(A)** Representative western blots with anti-Hsp70, anti-Htt-NT (stronger
553 recognition of wt-Htt), anti-polyQ (stronger recognition of expanded polyQ in mut-Htt),
554 and anti-ubiquitin; Coomassie: loading control. **(B)** Western blot quantification of Hsp70
555 levels; $n = 3$ independent experiments; Factorial ANOVA: $*P < 0.05$, heat shock effect;
556 $^{\S}P < 0.05$, mut-Htt effect. **(C)** Western blot quantification of ubiquitin-conjugated
557 proteins (Ub-proteins); $n = 3$ independent experiments; Factorial ANOVA: $^{\#}P < 0.05$. **(D,**
558 **E)** Western blot quantification of Htt levels; $n = 4$ independent experiments; Factorial
559 ANOVA: $^{\#}P < 0.05$.

560

561 **Figure 8: Putative model of mutant huntingtin effects on cellular proteostasis and**
562 **the mechanisms of action of YM-1. (A)** Mutant full-length Htt undergoes proteolysis
563 and generates N-terminal fragments containing the expanded polyQ tract. N-terminal Htt
564 fragments can oligomerize and form Htt aggregates [2, 3]. **(B)** N-terminal Htt fragments
565 disrupt the nuclear membrane by interacting with nucleoporins [52, 53], facilitating the
566 entry of N-terminal Htt to the nucleus where it aggregates. **(C)** The allosteric activator
567 YM-1 inhibits the ATPase domain of Hsp70, stabilizing Hsp70 in its ADP-bound
568 conformation, which has higher affinity for substrates. Thus, YM-1 delays the release of
569 Hsp70 substrates, favouring their ubiquitination by CHIP and subsequent proteasomal
570 degradation [17, 48]. **(D)** YM-1 accumulates in mitochondria where it interacts with the
571 mitochondrial Hsp70 - Grp75 - a subunit of the translocase of the inner mitochondrial
572 membrane (TIM) [54]. Stabilization of the Grp75 ADP-bound conformation by YM-1
573 slows down the substrate release, disturbing mitochondrial protein import, which can
574 increase the levels of NRF1 (nuclear factor erythroid 2-related factor 1; not to be confused
575 with nuclear respiratory factor 1) and induce proteasomal degradation [33, 34].

576

577

578 **References**

579

580 [1] S.J. Tabrizi, R. Ghosh, B.R. Leavitt, Huntingtin Lowering Strategies for Disease
581 Modification in Huntington's Disease, *Neuron*, 102 (2019) 899.

582 [2] G.P. Bates, R. Dorsey, J.F. Gusella, M.R. Hayden, C. Kay, B.R. Leavitt, M. Nance,
583 C.A. Ross, R.I. Scahill, R. Wetzel, E.J. Wild, S.J. Tabrizi, Huntington disease, *Nat Rev*
584 *Dis Primers*, 1 (2015) 15005.

585 [3] F. Saudou, S. Humbert, The Biology of Huntingtin, *Neuron*, 89 (2016) 910-926.

586 [4] T.R. Soares, S.D. Reis, B.R. Pinho, M.R. Duchen, J.M.A. Oliveira, Targeting the
587 proteostasis network in Huntington's disease, *Ageing Res Rev*, 49 (2019) 92-103.

588 [5] M.S. Hipp, P. Kasturi, F.U. Hartl, The proteostasis network and its decline in ageing,
589 *Nat Rev Mol Cell Biol*, 20 (2019) 421-435.

590 [6] S.D. Reis, B.R. Pinho, J.M.A. Oliveira, Modulation of Molecular Chaperones in
591 Huntington's Disease and Other Polyglutamine Disorders, *Mol Neurobiol*, 54 (2017)
592 5829-5854.

593 [7] R. Rosenzweig, N.B. Nillegoda, M.P. Mayer, B. Bukau, The Hsp70 chaperone
594 network, *Nat Rev Mol Cell Biol*, 20 (2019) 665-680.

595 [8] M. Ferraro, I. D'Annessa, E. Moroni, G. Morra, A. Paladino, S. Rinaldi, F.
596 Compostella, G. Colombo, Allosteric Modulators of HSP90 and HSP70: Dynamics Meets
597 Function through Structure-Based Drug Design, *J Med Chem*, 62 (2019) 60-87.

598 [9] A.K. Davis, W.B. Pratt, A.P. Lieberman, Y. Osawa, Targeting Hsp70 facilitated
599 protein quality control for treatment of polyglutamine diseases, *Cell Mol Life Sci*, 77
600 (2020) 977-996.

601 [10] I.V. Guzhova, V.F. Lazarev, A.V. Kaznacheeva, M.V. Ippolitova, V.I. Muronetz,
602 A.V. Kinev, B.A. Margulis, Novel mechanism of Hsp70 chaperone-mediated prevention
603 of polyglutamine aggregates in a cellular model of huntington disease, *Hum Mol Genet*,
604 20 (2011) 3953-3963.

605 [11] A. Sittler, R. Lurz, G. Lueder, J. Priller, H. Lehrach, M.K. Hayer-Hartl, F.U. Hartl,
606 E.E. Wanker, Geldanamycin activates a heat shock response and inhibits huntingtin
607 aggregation in a cell culture model of Huntington's disease, *Hum Mol Genet*, 10 (2001)
608 1307-1315.

609 [12] D.G. Hay, K. Sathasivam, S. Tobaben, B. Stahl, M. Marber, R. Mestrlil, A. Mahal,
610 D.L. Smith, B. Woodman, G.P. Bates, Progressive decrease in chaperone protein levels

611 in a mouse model of Huntington's disease and induction of stress proteins as a therapeutic
612 approach, *Hum Mol Genet*, 13 (2004) 1389-1405.

613 [13] T.M. Newton, J.A. Duce, E.D. Bayle, The proteostasis network provides targets for
614 neurodegeneration, *Br J Pharmacol*, 176 (2019) 3508-3514.

615 [14] J.L. Howarth, C.P. Glover, J.B. Uney, HSP70 interacting protein prevents the
616 accumulation of inclusions in polyglutamine disease, *J Neurochem*, 108 (2009) 945-951.

617 [15] R. Schlecht, S.R. Scholz, H. Dahmen, A. Wegener, C. Sirrenberg, D. Musil, J.
618 Bomke, H.M. Eggenweiler, M.P. Mayer, B. Bukau, Functional analysis of Hsp70
619 inhibitors, *PLoS One*, 8 (2013) e78443.

620 [16] V. Srinivasan, C. Bruelle, E. Scifo, D.D. Pham, R. Soliymani, M. Lalowski, D.
621 Lindholm, Dynamic Interaction of USP14 with the Chaperone HSC70 Mediates
622 Crosstalk between the Proteasome, ER Signaling, and Autophagy, *iScience*, 23 (2020)
623 100790.

624 [17] A.M. Wang, Y. Miyata, S. Klinedinst, H.M. Peng, J.P. Chua, T. Komiyama, X. Li,
625 Y. Morishima, D.E. Merry, W.B. Pratt, Y. Osawa, C.A. Collins, J.E. Gestwicki, A.P.
626 Lieberman, Activation of Hsp70 reduces neurotoxicity by promoting polyglutamine
627 protein degradation, *Nat Chem Biol*, 9 (2013) 112-118.

628 [18] J. Abisambra, U.K. Jinwal, Y. Miyata, J. Rogers, L. Blair, X. Li, S.P. Seguin, L.
629 Wang, Y. Jin, J. Bacon, S. Brady, M. Cockman, C. Guidi, J. Zhang, J. Koren, Z.T. Young,
630 C.A. Atkins, B. Zhang, L.Y. Lawson, E.J. Weeber, J.L. Brodsky, J.E. Gestwicki, C.A.
631 Dickey, Allosteric heat shock protein 70 inhibitors rapidly rescue synaptic plasticity
632 deficits by reducing aberrant tau, *Biol Psychiatry*, 74 (2013) 367-374.

633 [19] Z.T. Young, J.N. Rauch, V.A. Assimon, U.K. Jinwal, M. Ahn, X. Li, B.M. Dunyak,
634 A. Ahmad, G.A. Carlson, S.R. Srinivasan, E.R. Zuiderweg, C.A. Dickey, J.E. Gestwicki,
635 Stabilizing the Hsp70-Tau Complex Promotes Turnover in Models of Tauopathy, *Cell*
636 *Chem Biol*, 23 (2016) 992-1001.

637 [20] J.A. Klickstein, S. Mukkavalli, M. Raman, AggreCount: an unbiased image analysis
638 tool for identifying and quantifying cellular aggregates in a spatially defined manner, *J*
639 *Biol Chem*, 295 (2020) 17672-17683.

640 [21] H. Olzscha, O. Fedorov, B.M. Kessler, S. Knapp, N.B. La Thangue, CBP/p300
641 Bromodomains Regulate Amyloid-like Protein Aggregation upon Aberrant Lysine
642 Acetylation, *Cell Chem Biol*, 24 (2017) 9-23.

643 [22] A. Thiruvalluvan, E.P. de Mattos, J.F. Brunsting, R. Bakels, D. Serlidaki, L.
644 Barazzuol, P. Conforti, A. Fatima, S. Koyuncu, E. Cattaneo, D. Vilchez, S. Bergink, E.

645 Boddeke, S. Copray, H.H. Kampinga, DNAJB6, a Key Factor in Neuronal Sensitivity to
646 Amyloidogenesis, *Mol Cell*, 78 (2020) 346-358 e349.

647 [23] X. Cen, Y. Chen, X. Xu, R. Wu, F. He, Q. Zhao, Q. Sun, C. Yi, J. Wu, A. Najafov,
648 H. Xia, Pharmacological targeting of MCL-1 promotes mitophagy and improves disease
649 pathologies in an Alzheimer's disease mouse model, *Nat Commun*, 11 (2020) 5731.

650 [24] B.R. Pinho, S.D. Reis, R.C. Hartley, M.P. Murphy, J.M.A. Oliveira, Mitochondrial
651 superoxide generation induces a parkinsonian phenotype in zebrafish and huntingtin
652 aggregation in human cells, *Free Radic Biol Med*, 130 (2019) 318-327.

653 [25] T. Ratovitski, M. Nakamura, J. D'Ambola, E. Chighladze, Y. Liang, W. Wang, R.
654 Graham, M.R. Hayden, D.R. Borchelt, R.R. Hirschhorn, C.A. Ross, N-terminal
655 proteolysis of full-length mutant huntingtin in an inducible PC12 cell model of
656 Huntington's disease, *Cell Cycle*, 6 (2007) 2970-2981.

657 [26] M. Czeredys, J. Gruszczynska-Biegala, T. Schacht, A. Methner, J. Kuznicki,
658 Expression of genes encoding the calcium signalosome in cellular and transgenic models
659 of Huntington's disease, *Front Mol Neurosci*, 6 (2013) 42.

660 [27] P. Martine, A. Chevriaux, V. Derangere, L. Apetoh, C. Garrido, F. Ghiringhelli, C.
661 Rebe, HSP70 is a negative regulator of NLRP3 inflammasome activation, *Cell Death Dis*,
662 10 (2019) 256.

663 [28] A.V. Gomez, G. Cordova, R. Munita, G.E. Parada, A.P. Barrios, G.I. Cancino, A.R.
664 Alvarez, M.E. Andres, Characterizing HSF1 Binding and Post-Translational
665 Modifications of hsp70 Promoter in Cultured Cortical Neurons: Implications in the Heat-
666 Shock Response, *PLoS One*, 10 (2015) e0129329.

667 [29] B.R. Pinho, A.I. Duarte, P.M. Canas, P.I. Moreira, M.P. Murphy, J.M.A. Oliveira,
668 The interplay between redox signalling and proteostasis in neurodegeneration: In vivo
669 effects of a mitochondria-targeted antioxidant in Huntington's disease mice, *Free Radic*
670 *Biol Med*, 146 (2020) 372-382.

671 [30] T. Liu, C.K. Daniels, S. Cao, Comprehensive review on the HSC70 functions,
672 interactions with related molecules and involvement in clinical diseases and therapeutic
673 potential, *Pharmacol Ther*, 136 (2012) 354-374.

674 [31] J. Koren, 3rd, Y. Miyata, J. Kiray, J.C. O'Leary, 3rd, L. Nguyen, J. Guo, L.J. Blair,
675 X. Li, U.K. Jinwal, J.Q. Cheng, J.E. Gestwicki, C.A. Dickey, Rhodacyanine derivative
676 selectively targets cancer cells and overcomes tamoxifen resistance, *PLoS One*, 7 (2012)
677 e35566.

678 [32] S.W. Perry, J.P. Norman, J. Barbieri, E.B. Brown, H.A. Gelbard, Mitochondrial
679 membrane potential probes and the proton gradient: a practical usage guide,
680 *Biotechniques*, 50 (2011) 98-115.

681 [33] A. Northrop, H.A. Byers, S.K. Radhakrishnan, Regulation of NRF1, a master
682 transcription factor of proteasome genes: implications for cancer and neurodegeneration,
683 *Mol Biol Cell*, 31 (2020) 2158-2163.

684 [34] F. Boos, L. Kramer, C. Groh, F. Jung, P. Haberkant, F. Stein, F. Wollweber, A.
685 Gackstatter, E. Zoller, M. van der Laan, M.M. Savitski, V. Benes, J.M. Herrmann,
686 Mitochondrial protein-induced stress triggers a global adaptive transcriptional
687 programme, *Nat Cell Biol*, 21 (2019) 442-451.

688 [35] C.A. Ross, S.J. Tabrizi, Huntington's disease: from molecular pathogenesis to
689 clinical treatment, *Lancet Neurol*, 10 (2011) 83-98.

690 [36] S.J. Tabrizi, M.D. Flower, C.A. Ross, E.J. Wild, Huntington disease: new insights
691 into molecular pathogenesis and therapeutic opportunities, *Nat Rev Neurol*, 16 (2020)
692 529-546.

693 [37] A.P. Lieberman, V.G. Shakkottai, R.L. Albin, Polyglutamine Repeats in
694 Neurodegenerative Diseases, *Annu Rev Pathol*, 14 (2019) 1-27.

695 [38] G.P. Lotz, J. Legleiter, R. Aron, E.J. Mitchell, S.Y. Huang, C. Ng, C. Glabe, L.M.
696 Thompson, P.J. Muchowski, Hsp70 and Hsp40 functionally interact with soluble mutant
697 huntingtin oligomers in a classic ATP-dependent reaction cycle, *J Biol Chem*, 285 (2010)
698 38183-38193.

699 [39] E. Monsellier, V. Redeker, G. Ruiz-Arlandis, L. Bousset, R. Melki, Molecular
700 interaction between the chaperone Hsc70 and the N-terminal flank of huntingtin exon 1
701 modulates aggregation, *J Biol Chem*, 290 (2015) 2560-2576.

702 [40] R. Gomez-Pastor, E.T. Burchfiel, D.J. Thiele, Regulation of heat shock transcription
703 factors and their roles in physiology and disease, *Nat Rev Mol Cell Biol*, 19 (2018) 4-19.

704 [41] A.E. Masser, W. Kang, J. Roy, J. Mohanakrishnan Kaimal, J. Quintana-Cordero,
705 M.R. Friedlander, C. Andreasson, Cytoplasmic protein misfolding titrates Hsp70 to
706 activate nuclear Hsf1, *Elife*, 8 (2019).

707 [42] L. Le Breton, M.P. Mayer, A model for handling cell stress, *Elife*, 5 (2016).

708 [43] D.B. Mahat, H.H. Salamanca, F.M. Duarte, C.G. Danko, J.T. Lis, Mammalian Heat
709 Shock Response and Mechanisms Underlying Its Genome-wide Transcriptional
710 Regulation, *Mol Cell*, 62 (2016) 63-78.

711 [44] D.R. Shimshek, M. Mueller, C. Wiessner, T. Schweizer, P.H. van der Putten, The
712 HSP70 molecular chaperone is not beneficial in a mouse model of alpha-synucleinopathy,
713 PLoS One, 5 (2010) e10014.

714 [45] S. Watanabe, N. Ageta-Ishihara, S. Nagatsu, K. Takao, O. Komine, F. Endo, T.
715 Miyakawa, H. Misawa, R. Takahashi, M. Kinoshita, K. Yamanaka, SIRT1
716 overexpression ameliorates a mouse model of SOD1-linked amyotrophic lateral sclerosis
717 via HSF1/HSP70i chaperone system, Mol Brain, 7 (2014) 62.

718 [46] E. Kim, B. Wang, N. Sastry, E. Masliah, P.T. Nelson, H. Cai, F.F. Liao, NEDD4-
719 mediated HSF1 degradation underlies alpha-synucleinopathy, Hum Mol Genet, 25 (2016)
720 211-222.

721 [47] J. Labbadia, H. Cunliffe, A. Weiss, E. Katsyuba, K. Sathasivam, T. Seredenina, B.
722 Woodman, S. Moussaoui, S. Frentzel, R. Luthi-Carter, P. Paganetti, G.P. Bates, Altered
723 chromatin architecture underlies progressive impairment of the heat shock response in
724 mouse models of Huntington disease, J Clin Invest, 121 (2011) 3306-3319.

725 [48] Z. Li, F.U. Hartl, A. Bracher, Structure and function of Hip, an attenuator of the
726 Hsp70 chaperone cycle, Nat Struct Mol Biol, 20 (2013) 929-935.

727 [49] J.S. Steffan, N. Agrawal, J. Pallos, E. Rockabrand, L.C. Trotman, N. Slepko, K. Illes,
728 T. Lukacsovich, Y.Z. Zhu, E. Cattaneo, P.P. Pandolfi, L.M. Thompson, J.L. Marsh,
729 SUMO modification of Huntingtin and Huntington's disease pathology, Science, 304
730 (2004) 100-104.

731 [50] M.S. Hipp, C.N. Patel, K. Bersuker, B.E. Riley, S.E. Kaiser, T.A. Shaler, M.
732 Brandeis, R.R. Kopito, Indirect inhibition of 26S proteasome activity in a cellular model
733 of Huntington's disease, J Cell Biol, 196 (2012) 573-587.

734 [51] C. Landles, R.E. Milton, N. Ali, R. Flomen, M. Flower, F. Schindler, C. Gomez-
735 Paredes, M.K. Bondulich, G.F. Osborne, D. Goodwin, G. Salsbury, C.L. Benn, K.
736 Sathasivam, E.J. Smith, S.J. Tabrizi, E.E. Wanker, G.P. Bates, Subcellular Localization
737 And Formation Of Huntingtin Aggregates Correlates With Symptom Onset And
738 Progression In A Huntington'S Disease Model, Brain Commun, 2 (2020) fcaa066.

739 [52] F. Gasset-Rosa, C. Chillon-Marinas, A. Goginashvili, R.S. Atwal, J.W. Artates, R.
740 Tabet, V.C. Wheeler, A.G. Bang, D.W. Cleveland, C. Lagier-Tourenne, Polyglutamine-
741 Expanded Huntingtin Exacerbates Age-Related Disruption of Nuclear Integrity and
742 Nucleocytoplasmic Transport, Neuron, 94 (2017) 48-57 e44.

743 [53] J.C. Grima, J.G. Daigle, N. Arbez, K.C. Cunningham, K. Zhang, J. Ochaba, C.
744 Geater, E. Morozko, J. Stocksedale, J.C. Glatzer, J.T. Pham, I. Ahmed, Q. Peng, H.

745 Wadhwa, O. Pletnikova, J.C. Troncoso, W. Duan, S.H. Snyder, L.P.W. Ranum, L.M.
746 Thompson, T.E. Lloyd, C.A. Ross, J.D. Rothstein, Mutant Huntingtin Disrupts the
747 Nuclear Pore Complex, *Neuron*, 94 (2017) 93-107 e106.

748 [54] E.A. Moehle, K. Shen, A. Dillin, Mitochondrial proteostasis in the context of cellular
749 and organismal health and aging, *J Biol Chem*, 294 (2019) 5396-5407.

750 [55] L. Papa, D. Germain, Estrogen receptor mediates a distinct mitochondrial unfolded
751 protein response, *J Cell Sci*, 124 (2011) 1396-1402.

752 [56] L. Wrobel, U. Topf, P. Bragoszewski, S. Wiese, M.E. Sztolsztener, S. Oeljeklaus,
753 A. Varabyova, M. Lirski, P. Chroscicki, S. Mroczek, E. Januszewicz, A. Dziembowski,
754 M. Koblowaska, B. Warscheid, A. Chacinska, Mistargeted mitochondrial proteins activate
755 a proteostatic response in the cytosol, *Nature*, 524 (2015) 485-488.

756 [57] J. Steffen, M. Seeger, A. Koch, E. Kruger, Proteasomal degradation is
757 transcriptionally controlled by TCF11 via an ERAD-dependent feedback loop, *Mol Cell*,
758 40 (2010) 147-158.

759 [58] A. Neueder, T.A. Gipson, S. Batterton, H.J. Lazell, P.P. Farshim, P. Paganetti, D.E.
760 Housman, G.P. Bates, HSF1-dependent and -independent regulation of the mammalian
761 in vivo heat shock response and its impairment in Huntington's disease mouse models,
762 *Sci Rep*, 7 (2017) 12556.

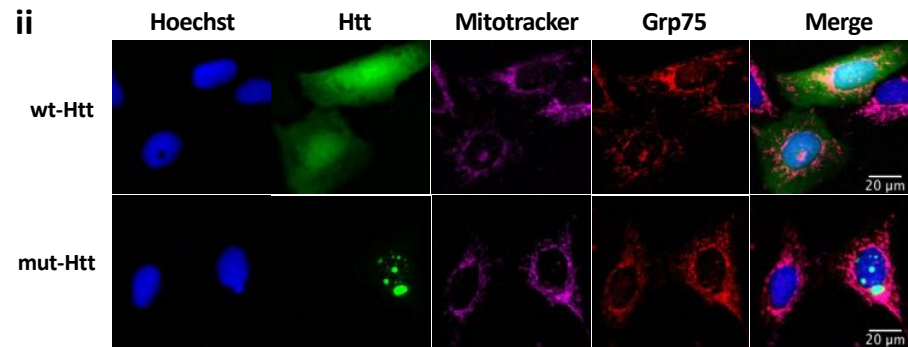
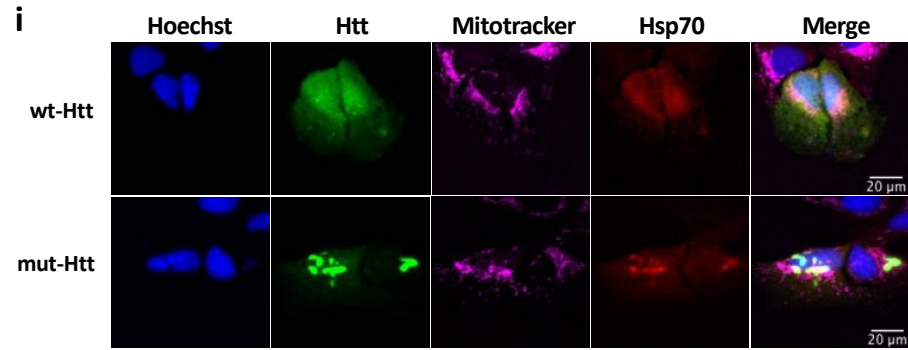
763 [59] W.B. Pratt, J.E. Gestwicki, Y. Osawa, A.P. Lieberman, Targeting Hsp90/Hsp70-
764 based protein quality control for treatment of adult onset neurodegenerative diseases,
765 *Annu Rev Pharmacol Toxicol*, 55 (2015) 353-371.

766

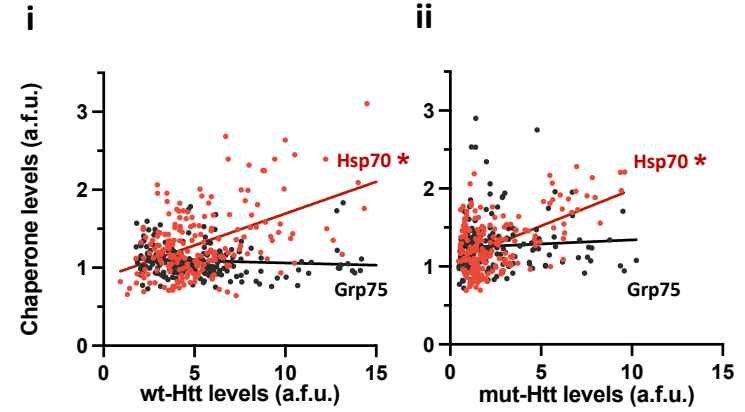
767

Figure 1

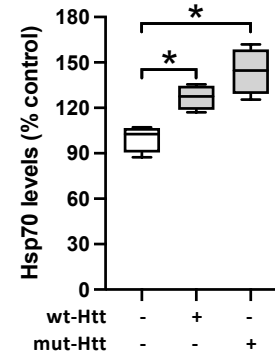
A



B



C



D

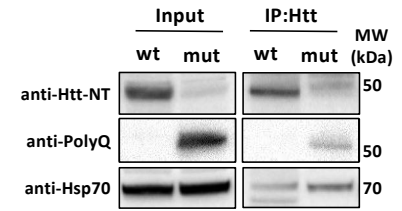
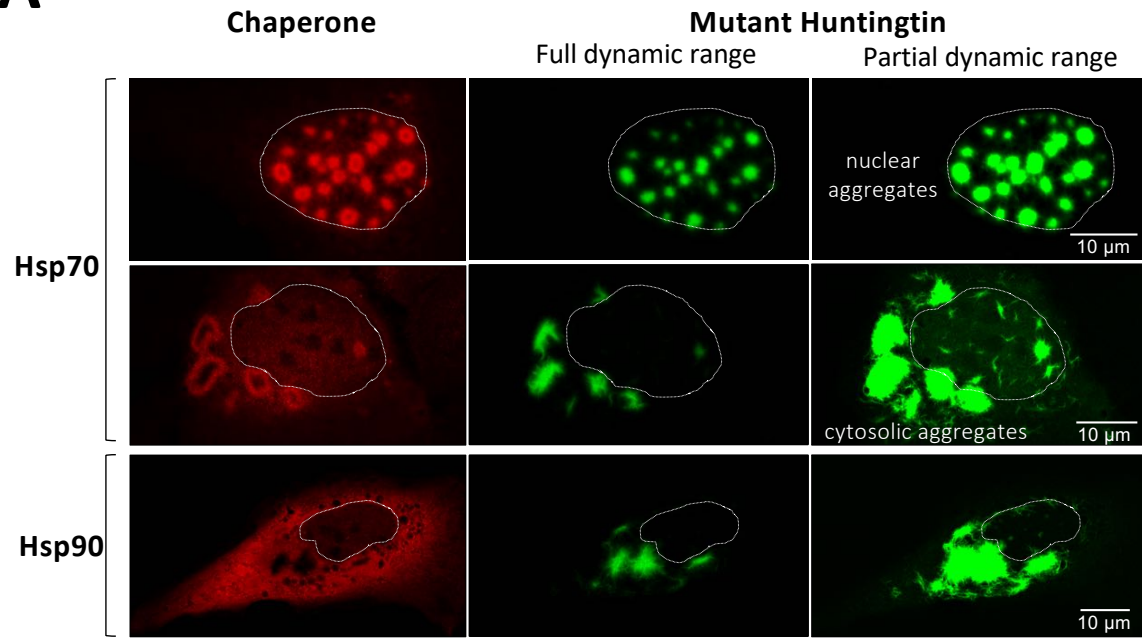
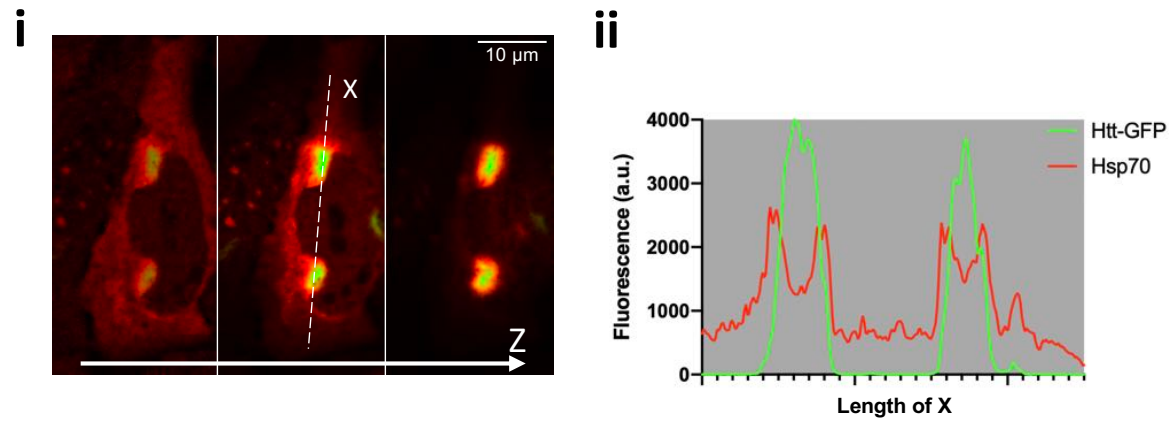


Figure 2

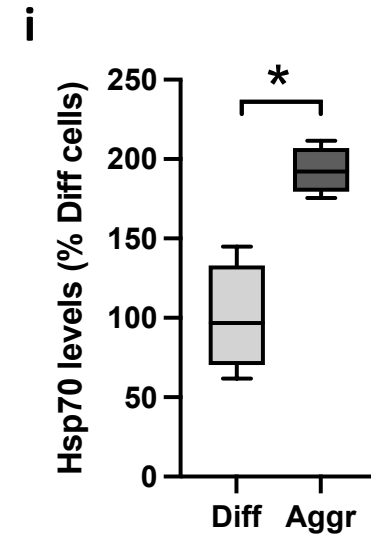
A



B



C



ii

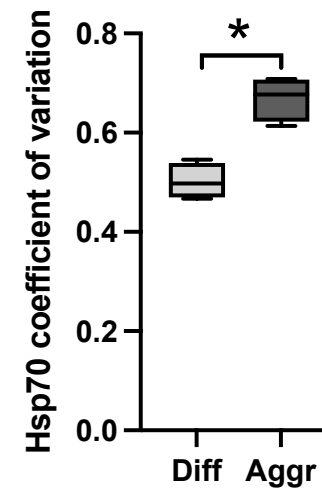


Figure 3

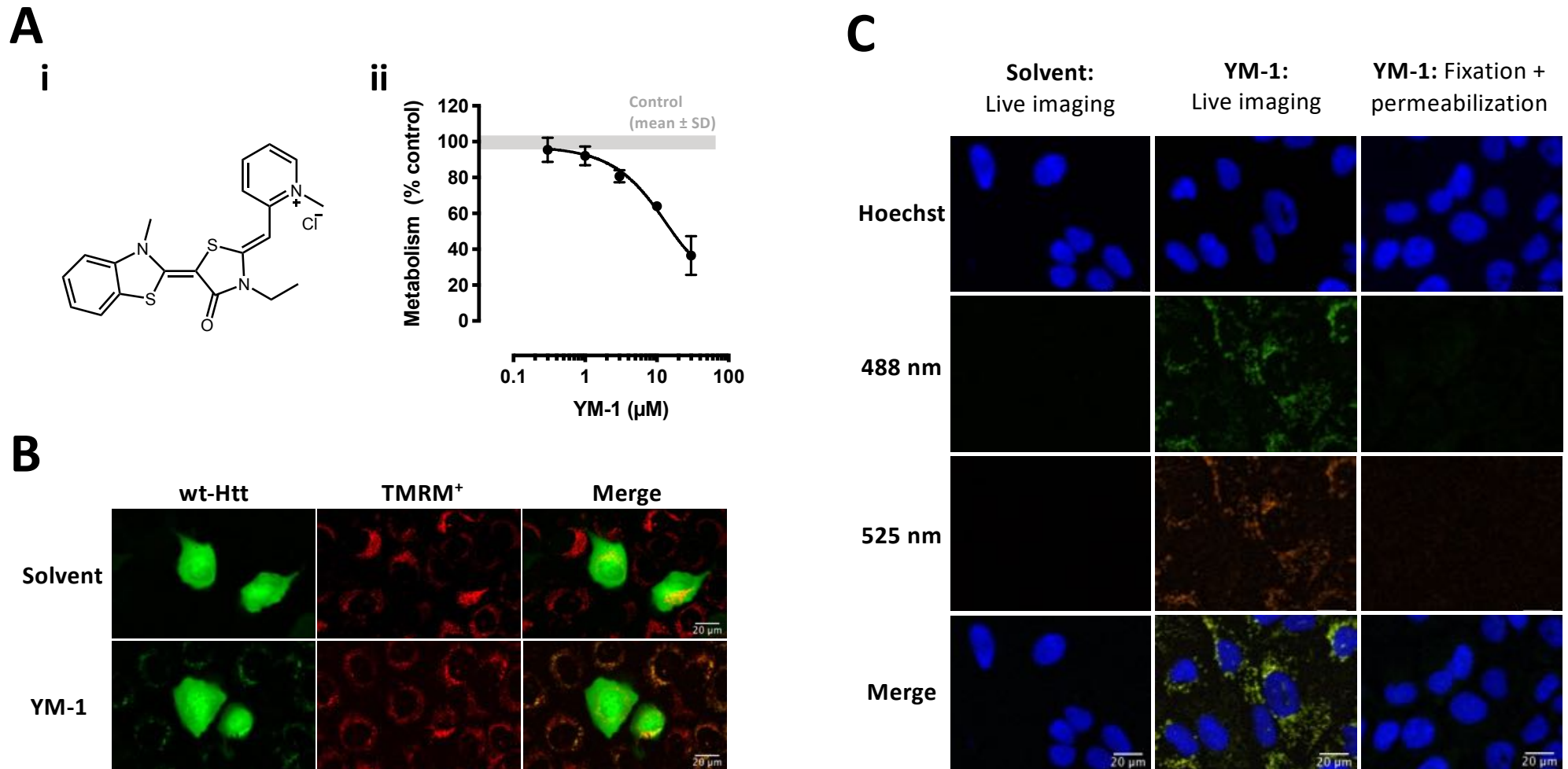


Figure 4

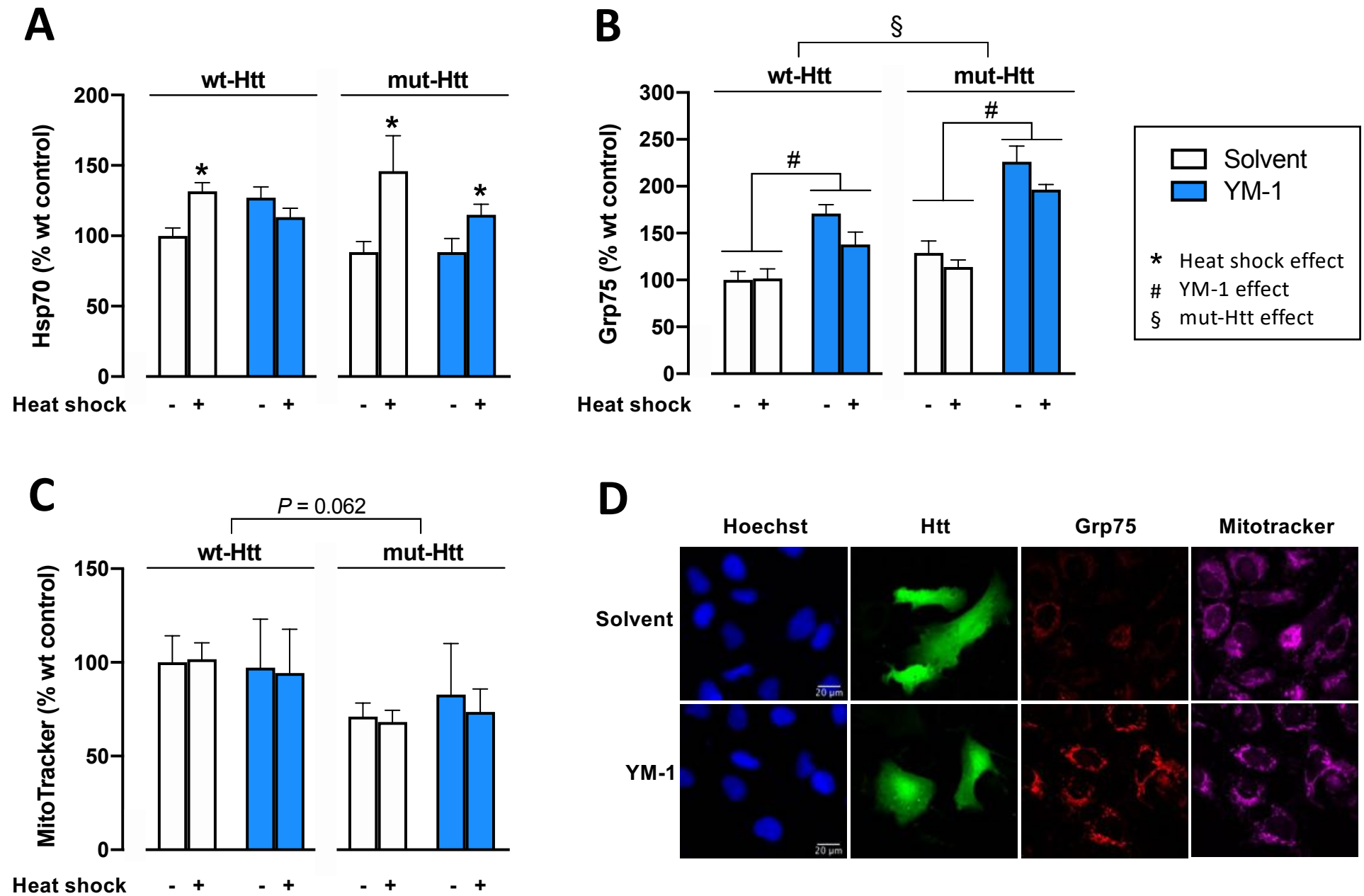
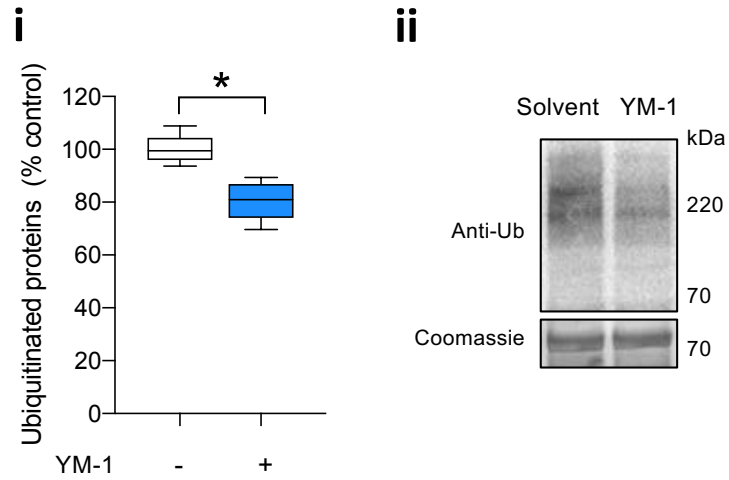
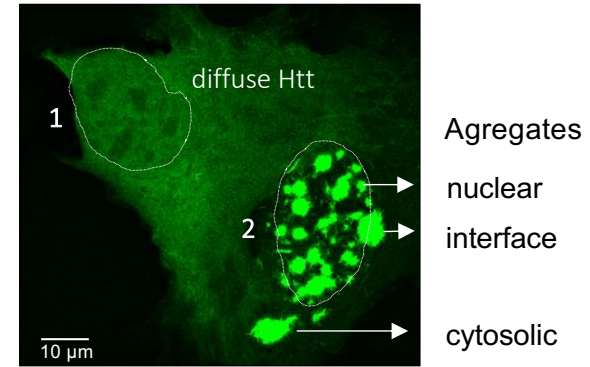


Figure 5

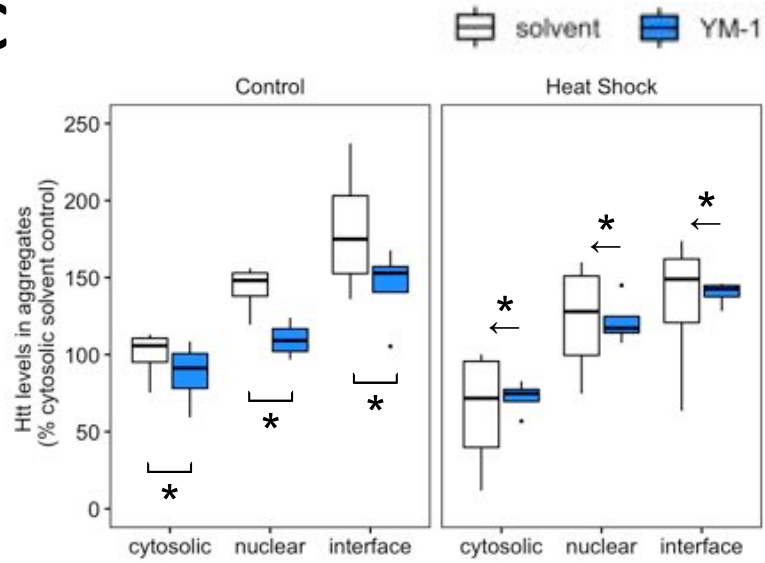
A



B



C



D

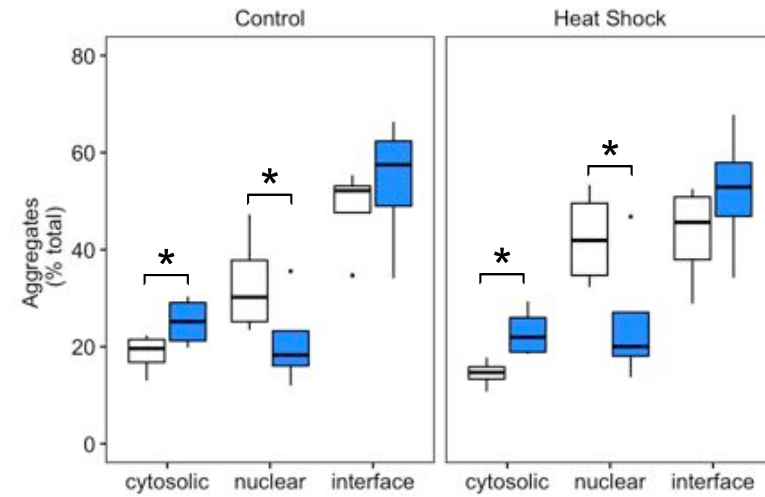
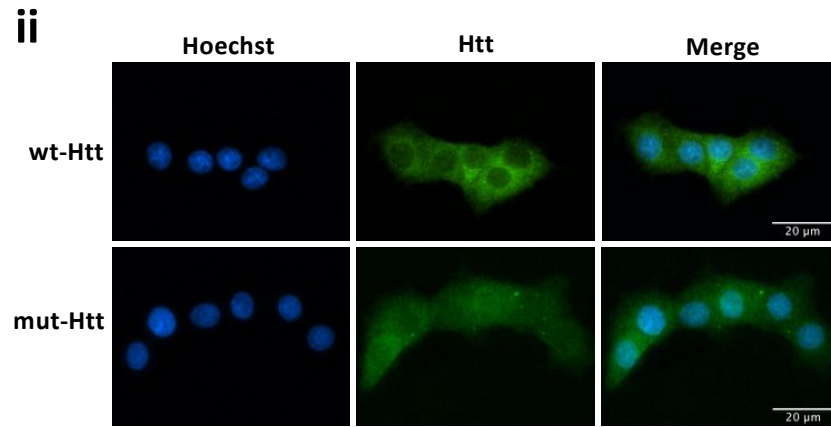
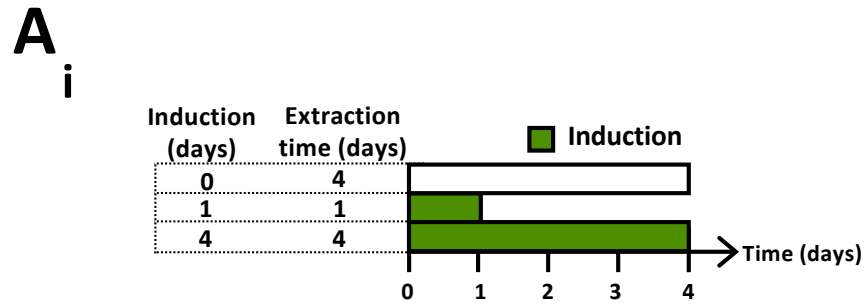
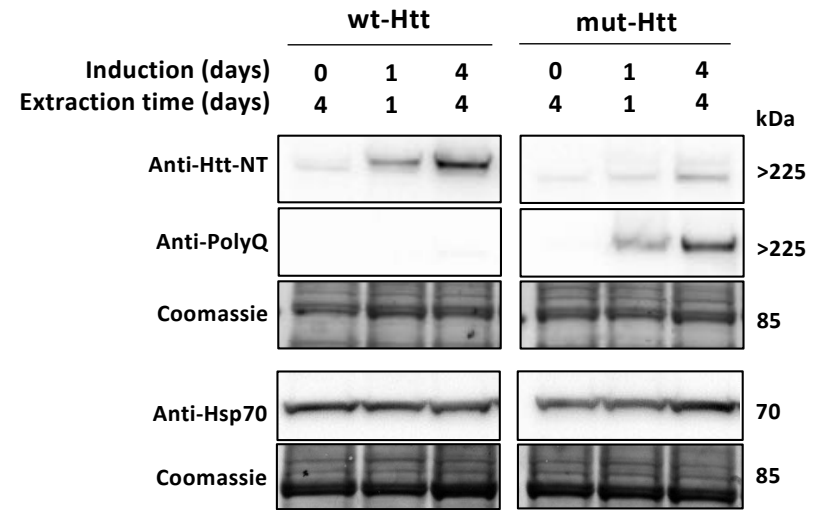


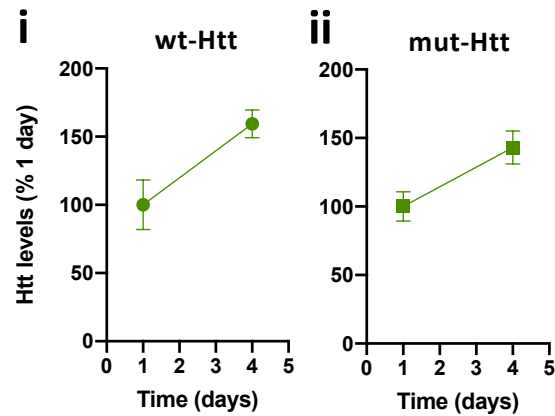
Figure 6



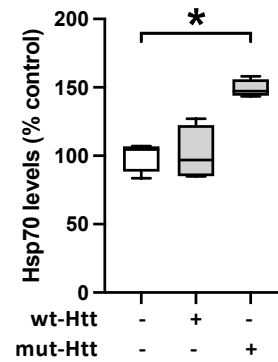
iii



B



C



D

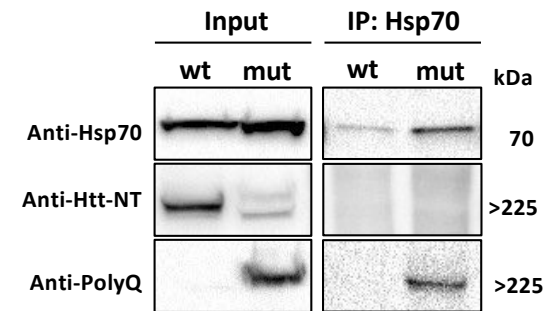


Figure 7

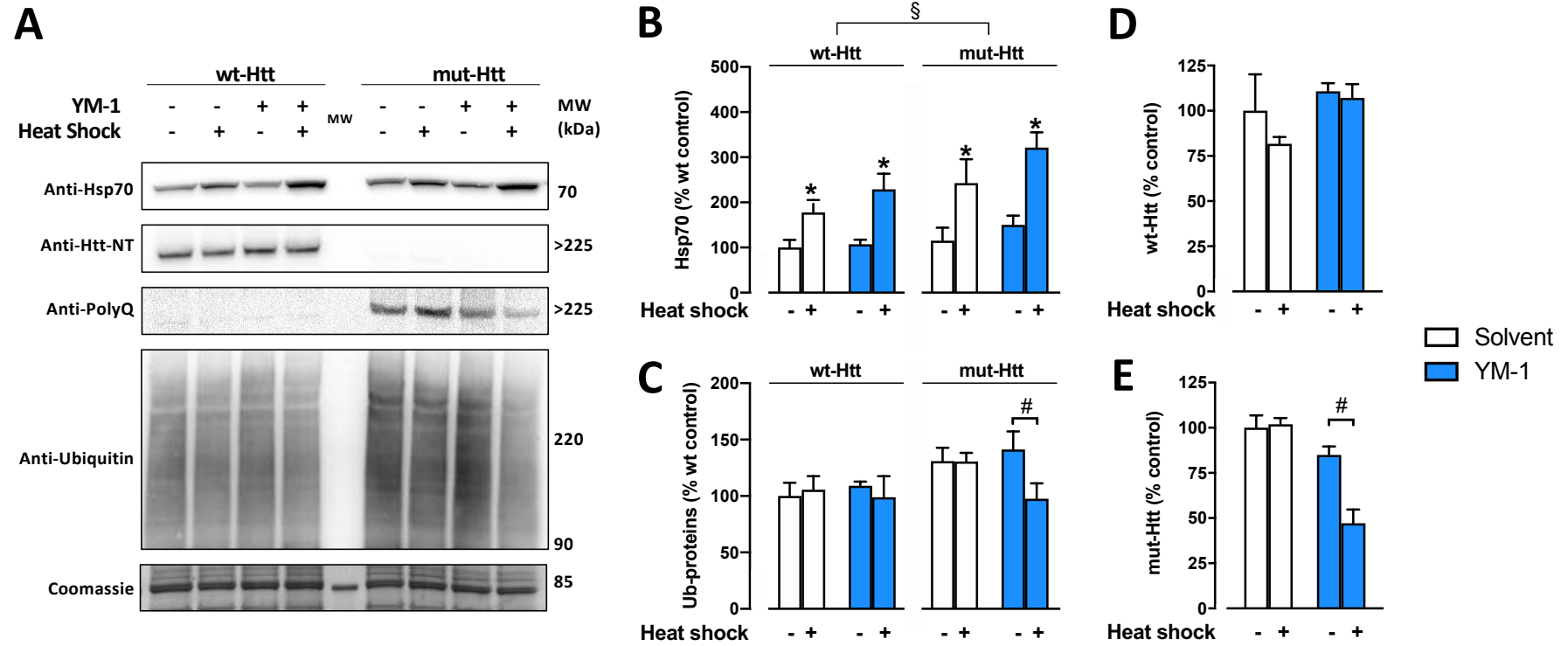
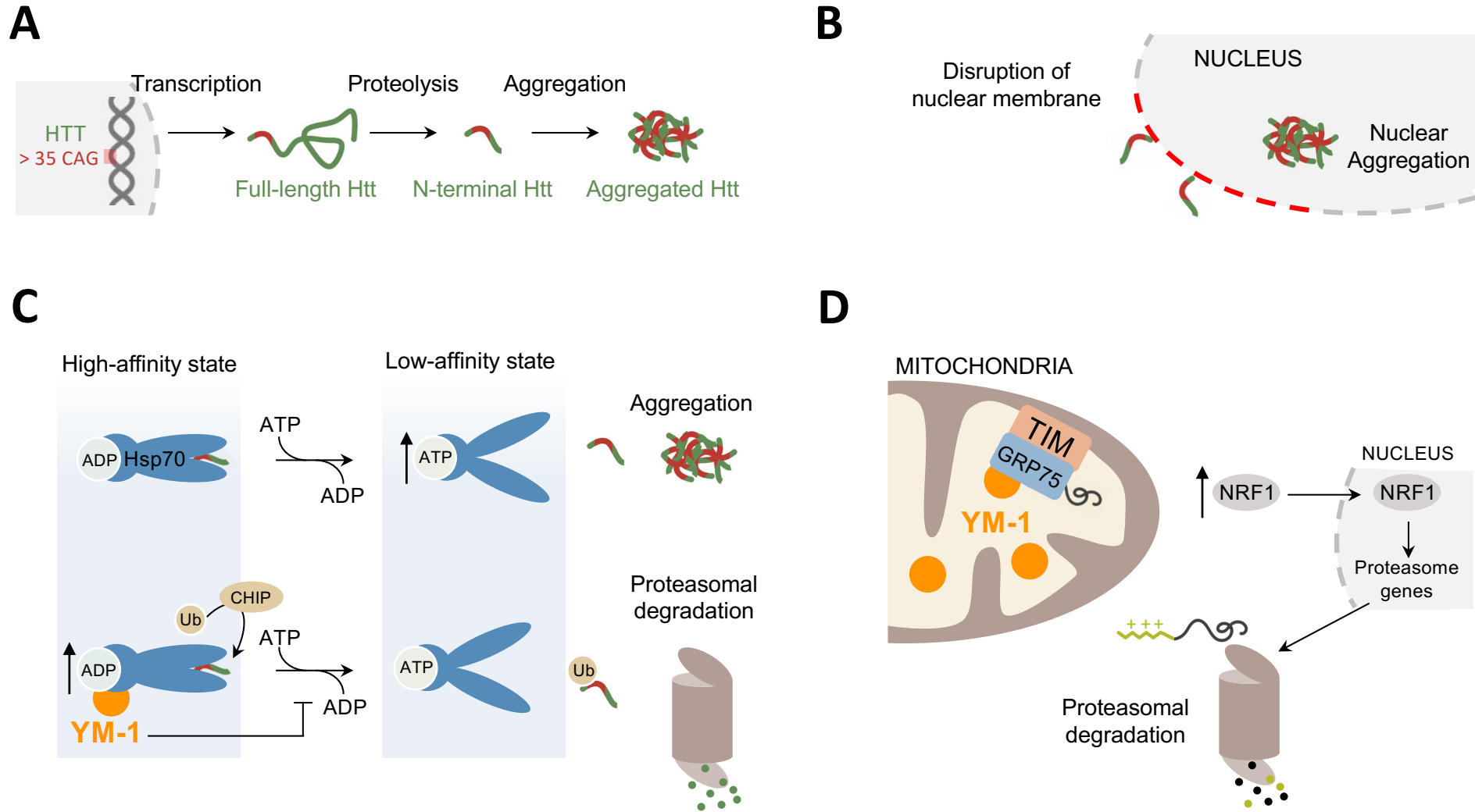
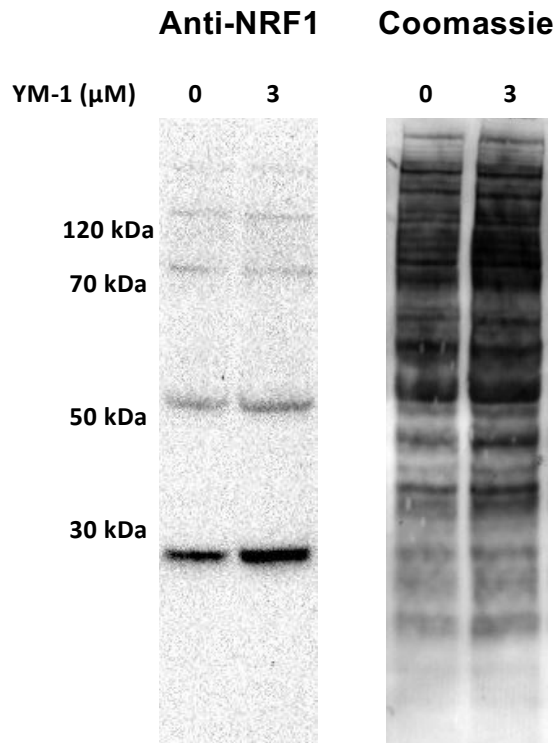
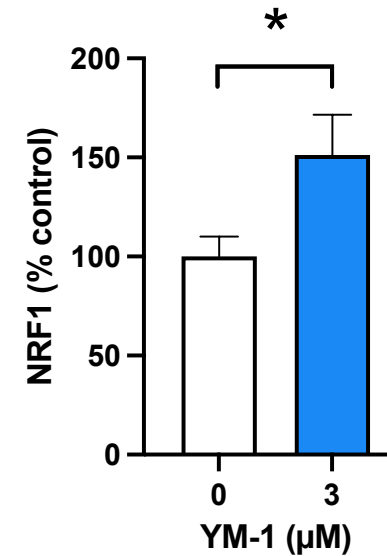


Figure 8



A**B**

Supplementary Figure 1. YM-1 increases the levels of NRF1. PC12 cells with inducible expression of N-terminal huntingtin fragment containing 74 polyglutamine repeats (Wytenbach et al. 2001; DOI: 10.1093/hmg/10.17.1829) were simultaneously treated with doxycycline (to induce huntingtin expression) and solvent/YM-1 for 48h. Levels of NRF1 (nuclear factor erythroid 2-related factor 1; not to be confused with nuclear respiratory factor 1) were quantified by western blot using the primary antibody anti-NRF1 (1:500; sc-28379; Santa Cruz Biotechnology) and membrane staining with coomassie was used for protein loading control. **(A)** Representative blot. **(B)** NRF1 levels (sum of detected NRF1 isoforms) in percentage of cells treated with solvent (control); $n = 3$ independent experiments; $*P < 0.05$, ratio paired t -test.